



INTERNATIONAL JOURNAL OF RESEARCH IN MEDICAL
SCIENCES & TECHNOLOGY

e-ISSN:2455-5134; p-ISSN: 2455-9059

GREEN SYNTHESIS OF SILVER NANOPARTICLE USING GREEN
TEA LEAVES EXTRACT FOR REMOVAL CIPROFLOXACIN (CIP)
FROM AQUEOUS MEDIA

***Fatimah Q. Kadhim, *Mohammed A. Atiya, **Ahmed K. Hassan**

*Al-Khwarizmi College of Engineering, University of Baghdad, Baghdad,
Iraq

**Ministry of Science and Technology, Baghdad, Iraq

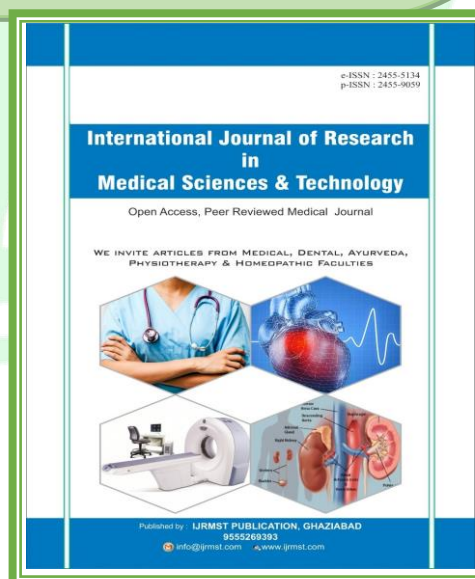
Paper Received: 13th April, 2021; **Paper Accepted:** 03rd May, 2021;

Paper Published: 29th June, 2021

DOI: <http://doi.org/10.37648/ijrmst.v11i01.008>

How to cite the article:

Fatimah Q. Kadhim, Mohammed A.
Atiya1, Ahmed K. Hassan, Green
Synthesis of Silver Nanoparticle Using
Green Tea Leaves Extract for Removal
Ciprofloxacin (CIP) From Aqueous
Media, IJRMST, January-June 2021,
Vol 11, 74-99, DOI:
<http://doi.org/10.37648/ijrmst.v11i01.008>



ABSTRACT

This study examines the removal of ciprofloxacin in an aqueous solution using green tea silver nanoparticles (Ag-NPs). The synthesized Ag-NPs have been classified by the different techniques of SEM, AFM, BET, FTIR, and Zeta potential. Spherical nanoparticles with average sizes of 32 nm and a surface area of 1.2387m²/g are found to be silver nanoparticles. The results showed that the ciprofloxacin removal efficiency depends on the initial pH (2.5-10), CIP (2-15 mg/L), temperature (20-50°C), time (0-180 min), and Ag-NPs dosage (0.1-1g/L). Batch experiments revealed that the removal rate with ratio (1:1) (w/w) were 52%, and 79.8% of the 10 mg/L of CIP at 60, and 180 minutes, respectively with optimal pH=4. Kinetic models for adsorption and ciprofloxacin mechanism removal were also investigated, and kinetic analyzes showed adsorption to be a 3.8727kJ.mol⁻¹ activation energy physical adsorption mechanism. The kinetic removal process, due to the low activation energy of 14.0606kJ.mol⁻¹, is preferred the model of first-order after a physical diffusion-controlled reaction. Adsorption information from Langmuir, Freundlich, Temkin, and Dubinin models was followed, and the Dubinin isotherm model was the best-fitted model. the thermodynamic parameter ΔG^0 values at 20, 30, 40 and 50°C were (0.5163, -0.0691, -0.9589, -0.5927kJ/mol). The value of ΔH^0 and ΔS^0 were (12.713kJ/mol and 0.0422073kJ/mol.k) which indicated favorable and endothermic sorption. The presence and concentration of CIP in aqueous media were identified through UV analysis.

Keywords: Green tea, Ciprofloxacin, Adsorption, Kinetics, Isotherm, Thermodynamics

INTRODUCTION

An increased risk to health due to indiscriminate disposal of medicinal products in aqueous environments and the infection of drugs in the soil was a significant concern due to damaging environmental consequences [1]. Pollution by drug waste from water supplies is currently one of the largest environmental issues faced by communities, especially in drinking resources [2][3]. In environmental media, for instance, excess medicines can be dangerous because they can change the situation of a natural ecosystem [4] [5]. Large amounts of

antibiotics are also used to treat many humans, animal, pig, and fish bacterial diseases as they are very effective[6] [7] [8]. Ciprofloxacin is widely used for a variety of global bacterial conditions as a therapeutic agent among many types of antibiotics [9][10][11]. In aqueous environments in the range 1-100 mg/L Fluoroquinolone was typically detected [12].

Ciprofloxacin is the commonly used broad-spectrum antibiotic agent of fluoroquinolone families {(1-cyclopropyl-6-fluoro-4-oxo-7-(piperazine-1-yl)-1, 4-dihydroquinoline-3-carboxyl acid

hydrochloride}}[12]. Uncertain disposal of pharmaceutical wastewater which loads antibioticly is dangerous for non-target human beings and biota as it may contain acute, contact-relating toxic, carcinogenic, and fatal errors [13][14][15]. Nevertheless, several studies have shown that chlorination of antibiotic wastewater in final treatment phases can detect and disinfect by-product chemicals that are considered carcinogenic. It is therefore essential to reduce antibiotic compounds to the permissible limit before being dumped in water systems (Balcioglu and Otker, 2004). Their environmental stability and extensive degradation periods typically categorize antibiotics and conventional processes do not eliminate them [16]. Efficient and advanced technologies are required to manage wastewater from antibiotics and the adsorption process is an effective, simple, and advanced universal treatment system which is one of the most promising approaches. The process uses natural and synthesized material (sorbents, adsorbents, bio-sorbents) to reduce contaminated solutions by contaminated pollutant molecules (adsorbates) [17][18].

In the field of nanotechnology, it is essential to develop environmentally friendly and reliable technology for the synthesis of metal nanoparticles. In addition to its unique properties and

applications in different areas such as medicine, catalysts, water treatment, nanoelectronics, pollution, and textiles, the researchers pay attention to silver nanoparticles. Different chemical and physical methods synthesize the silver nanoparticles. Synthesizers are costly, and many toxic chemicals are used as the biggest inconvenience of chemical and physical methods. Green nanotechnology plays an important role in the synthesis of silver nanoparticles to overcome these problems. Use of different plants for synthesizing nanoparticles of biogenic silver known as Green Nanoparticles [19]. Green synthesis methods have become simple alternates to chemical synthesis by utilizing biological micro-organisms and plant extracts, and green synthesis overcomes chemical approaches because it can be extended to a large scale in environmental friendliness, cost-effectiveness, and facility.

Ag-NPs are particularly outstanding for their excellent optical, thermal, catalytic, electromagnetic, adsorbent, and antimicrobial properties, which greatly differ from silver's volumetric properties. This is due to a decrease in size, which increases the area of the surface by volume and the nanoparticle's form [20] [21]. Furthermore, the mechanism of

competitive removal of some antibiotics during the sorption process should be investigated in the adsorption studies. Because of their strong biocidal action against microbial types, which have been used for many centuries to prevent and treat various diseases, particularly infections, silver nanoparticles, are one of the most universally used antimicrobials in biology and medicine [22]. The increased use of (Ag-NPs) in a different method of water treatment is due to its apparent potential as a disinfectant, in combination with filtration methods that do not produce by-products of disinfection (DBP) into the treated water [23].

The adsorption kinetics was obtained using the following models: the pseudo-first-order, the pseudo-second-order [24], [25], [26]. Elovich [27] [28], and Behnajady-Modirshahla-Ghanbary

(BMG) models [29]. The uptake analysis of CIP was studied by applying the Langmuir, Freundlich, Temkin, and Dubinin-Radushkevich models [30] [31], [24], and the thermodynamic parameters were also examined [27][31], [24], [30].

This work aimed to investigate the removal of a drug (Ciprofloxacin) from polluted water by adsorption technique using green tea silver nanoparticle.

MATERIALS AND METHODS

Chemicals Used

The ciprofloxacin used in this study was provided by the Ministry of Industry (Ibn Sine Center), and Table 1 highlights the characteristics of the drug. The maximum wavelength λ (nm) was measured using a spectrophotometer (UV/VIS model 1800 SHIMADZU).

Table 1: Main physical and chemical characteristics of Ciprofloxacin (CIP) used in this study [32], [33].

Drug class	Fluoroquinolone
IUPAC Name	1-Cyclopropyl-6-fluoro-4-oxo-7-(piperazin-1-yl)-1,4-dihydroquinoline-3-carboxylic acid hydrochloride hydrate
Molecular formula	C ₁₇ H ₂₁ ClFN ₃ O ₄
Molecular weight (g/mol)	385.82
Color	White
Purity	99.8%
λ_{max} (nm)	276

Adsorbent Preparation

The Ag-NPs nanoparticles were prepared using a similar procedure described in previous studies [34] [35] with some modifications.

The green tea extract was produced in 300 ml of distilled water by weighing 20.0 g of green tea (Lipton brand). The heat was applied to a hot plate for 30 minutes at 85 ° C. The extract was filtered with a membrane filter of 0.45 µm to remove the tea suspended particles and stored for further use in the refrigerator at 5 ° C. By adding 3.4g of AgNO₃ solids in 200 mL of distilled water, a 0.10 M AgNO₃ solution was prepared. This solution was then filtered by a membrane filter of 0.45 µm to remove any impurity after complete dissolution. The tea extract was then mixed with 0.10 M AgNO₃ and slowly added at room temperature for 15 minutes and constantly agitated. After the addition, the solution color was changed from colorless to brownish yellow, dark-brown precipitation was formed after five minutes, and after 30 min the color change to black. The color alteration is outstanding to the surface plasmon resonance exhibited by the metal nanoparticles and the reduction of silver nanoparticles. GT was used as a reducing and stabilizing agent to reduce the Silver ion Ag⁺ to Silver Nanoparticles Ag⁰ and

sorbitol as a capping and stabilizing agent. Following that, drop by drop 0.1 M of NaOH solution was added until the pH was adjusted to 9 [36][37].

The black precipitation of silver particles was collected using filter paper (Whatman No 1) by vacuum filtration and rinsed quickly with distilled water and ethanol several times to remove unresponding particles. The nanoparticles of the Ag-NPs were dried overnight at 60 ° C in the oven, then ground to a thin powder.

Characterization

Scanning Electron Microscopy images (SEM) were conducted using a TESCAN-Vega3 model to distinguish Ag-NPs, and they also helped identify alterations in the surface morphology due to adsorbent syncretization or adsorption processes. The functional groups present on the Ag-NPs, and their importance in the removal process, were detected by a Shimadzu FTIR spectroscopy instrument (Japan). These analyses were performed in the 400 to 4000 cm⁻¹ area of the wavenumber, as all well-known agricultural adsorbent groups are in this range. The basic GT-surface area was being analyzed. A zeta potential analysis was applied to detect nanoparticle stability and atomic force microscopy (AFM) was used to measure the size and surface

morphology of the nanoparticles and the contact force between the tip and the surface was calculated using a Brunauer–Emmett–Teller (BET) application, and a 120 mg Ag-NPs sample was then transferred to the BET tube (inner diameter=0.7 cm) and degassed in a vacuum for 24 hours at 60 °C before being analyzed. A zeta potential analysis was applied to detect nanoparticle stability and atomic force microscopy (AFM) was used to measure the size and surface morphology of the nanoparticles and the contact force between the tip and the surface.

Adsorption experiment of Ag- NPs

A work solution of 10 mg / L CIP has been dissolved by dissolving 0.01 g CIP in 1 L of distilled water and adjusting the pH of a solution before adding nanoparticles. Batch testing has been conducted for assessing the efficiency of CIP removal in this study. These experiments met several work parameters, including pH within 2 to 10, Ag-NPs 0.1 to 1 g/L, contact duration up to 180 min, original CIP antibiotic concentrations of 2 to 15 mg / L, and temperatures between 20 and 50 ° C. The experiments were carried out in two different ways. A special quantity of Ag-NPs was added to the CIP antibiotic solution and then stirred in a closed system

at 300 rpm. The pH solutions of 0.1 M H₂SO₄ and 0.1 M NaOH were adjusted and maintain the temperature to optimize the value of each parameter. During adsorption experiments, 10 mL samples were taken for analysis at various intervals. The initial CIP concentrations were calibrated using a 1 cm quartes container with the absorption of 276 nm wavelengths immediately after each sample with a spectrometer of UV / VIS. Nanoparticles of reference (blank) Ag-NPs solutions with the same concentrations as samples were read before each measurement. Adsorption data on temperature effects and contact times were used, particularly in thermodynamic, kinetic, isothermal studies, at different start concentrations and sorbent doses. Ag-NPs for the elimination of antibiotic contaminants of water solutions were evaluated based on their efficiency of removal (R %) and the adsorbent capacity (q_e mg / g) values [38][39]. The following two formulas calculated this:

$$R \% = (C_0 - C_t) * 100 / C_0$$

..... (1)

$$q_e = (C_0 - C_e) * V / W$$

..... (2)

Where, C₀, C_t, and C_e denote the initial, after a specific time of adsorption and equilibrium concentration of CIP aqueous

phase antibiotics (mg/L), respectively, V is the antibiotic solution volume in liters and W is the weight of adsorbent in (g).

RESULTS AND DISCUSSION

Characterization of Ag-NPs

1. Scanning electron microscopy (SEM) of Ag-NPs

The structure and composition of the synthesized silver nanoparticles Fig.1 were analyzed in the Scanning Electron Microscopy. The typical SEM picture

shows that the product mainly consists of spherical particles and a monodispersed distribution range of particles between 15 nm and 40 nm. Fig.1 shows that these silver nanoparticles (Ag-NPs) are installed by smaller, highly uniform nanoparticles with an average diameter of about 20 nm. SEM images demonstrated that most silver nanoparticles are mostly spherical, with a smooth surface and a well different with closed arrangement structure.

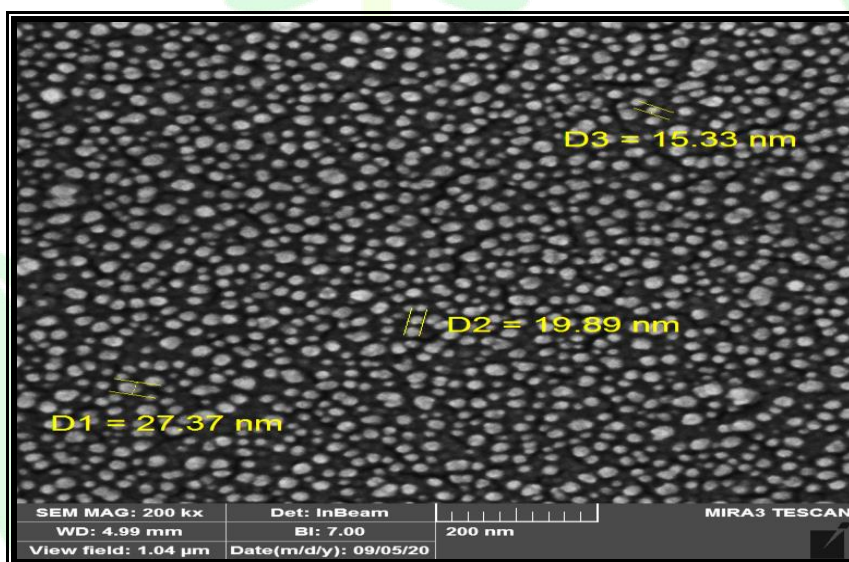


Fig.1: SEM micrograph of Ag-NPs

2. FTIR analysis of Ag-NPs

To determine the possible FTIR measurement, nanoparticles synthesized with extract tea leaf biomolecules responsible for copping and reducing agent of the Ag metal. 3271 cm^{-1} , 1637 cm^{-1} and 386 cm^{-1} are visible infrareds Fig.2. The N-H and O-H stretching of the protein connection is caused by the intense wide band at 3271 cm^{-1} . Wide and high absorption peaks between $3371\text{-}3259\text{ cm}^{-1}$, which showed the extending hydroxyl vibrations (O-H) were observed, which indicates the presence of polyphenols. The medium-intended band at 1637 cm^{-1} is produced by the mode C = O in amine I that is commonly found in the protein and

indicates that proteins are present as capping of silver nanoparticles that improve the stability of the synthesized nanoparticles. The intensive and wide peak, however, at 386 cm^{-1} , was equivalent to Ag metal [40].

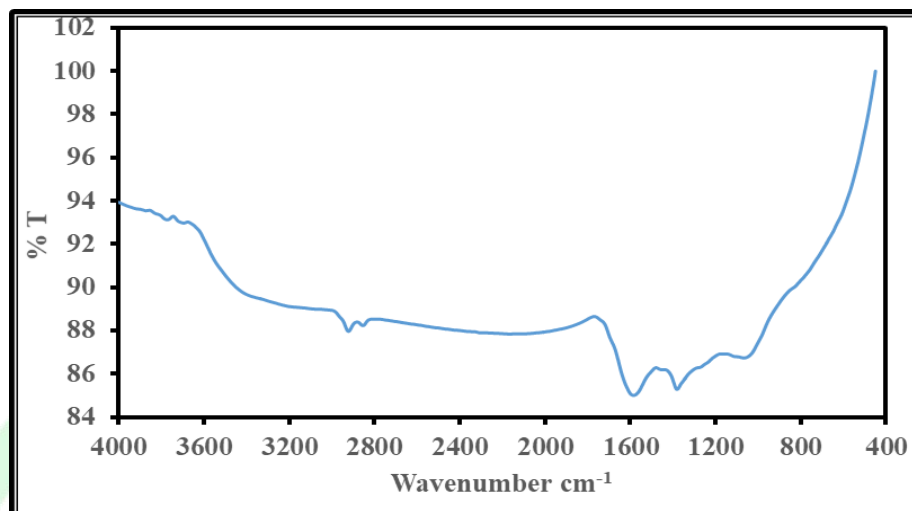


Fig.2: FTIR spectrum of Ag-NPs

3. Atomic Force Microscopy (AFM) of Ag-NPs

Atomic Force Microscopy (AFM) analysis was used for studying the average size and surface structure of the silver nanoparticles. In Fig.3-a particle size distribution of synthesizing silver nanoparticles shows the average size of less than 32 nm with no obvious agglomeration. Fig.3-b illustrates Ag-NPs surface morphology as nanoparticles

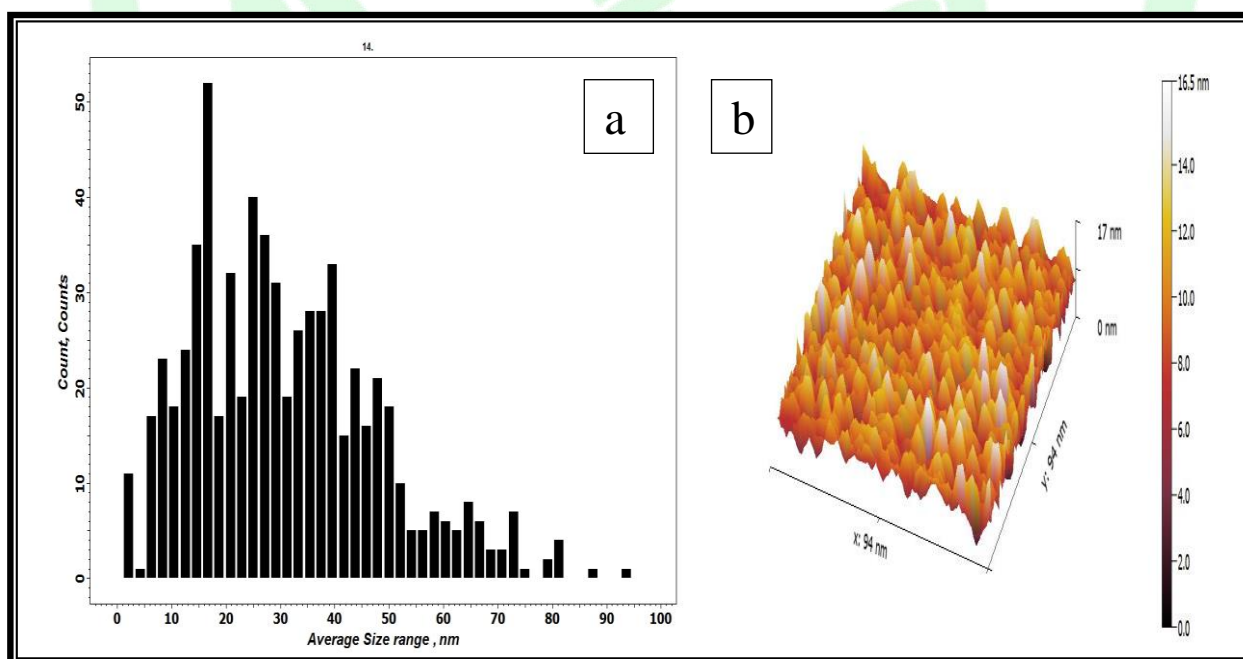


Fig.3: (a) Atomic Force Microscopy of Ag-NPs nanoparticles, (b) Ag-NPs surface morphology

4. Zeta potential analysis

The zeta potential analysis technique is used to identify the stability of the nanofluids. Zeta potential value for silver nanoparticles Fig. 4 was -29.1mV. The negative zeta potential values were attributed to the negative charge of green tea polyphenols. This result shows the presence of polyphenols on the surface of

nanoparticles [41]. The electrostatic repulsive forces between the negative-charged nanoparticles can prevent aggregation, thereby enhancing stability [42]. The zeta potential value $> \pm 60$ mV is excellent stability concerning the stability of nanoparticles in ambient fluid, good stability in $\pm (40-60)$ mV, stable in $\pm (30-40)$ mV, highly agglomerated in $< \pm 30$ mV.

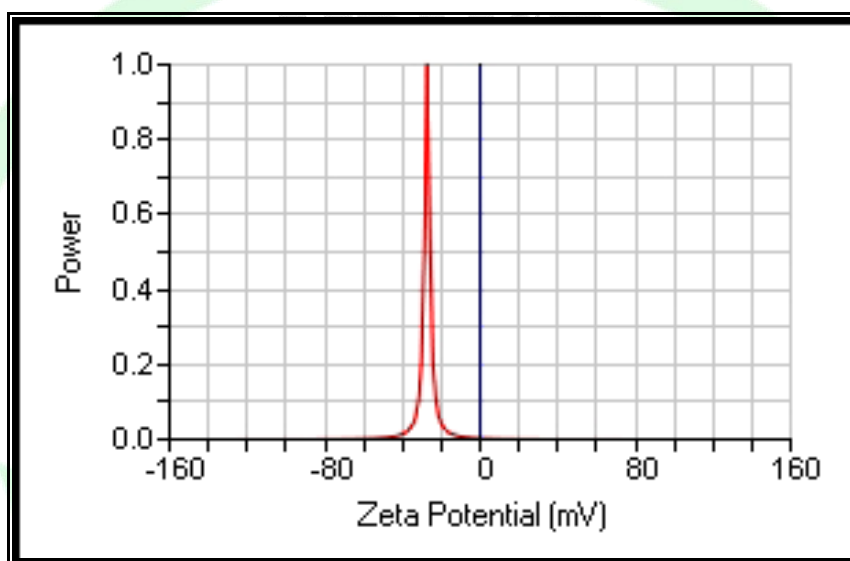


Fig.4: Zeta potential of Ag-NPs nanoparticles

5. Blumenauer-Emmer-Teller (BET) of Ag-NPs

Table 2 refers to Blumenauer-Emmer-Teller (BET) results that describe and clarify the surface area. In this analysis, the pore size was 5.1843 nm. According to the IUPAC, a pore size in the range of < 20 nm indicates supermicroporous.

Table 2: Blumenauer-Emmer-Teller parameter for Ag-NPs nanoparticles

Parameter	Value
BET (m ² /g)	1.2387
Pore volume(cm ³ /g)	0.000618
Pore size (nm)	5.1843

Removal of CIP at different condition

In a closed system, silver nanoparticles (Ag-NPs) were tested for removal of CIP, and various experimental conditions were used to measure removal efficiencies. Using UV-Vis at 276 nm wavelength samples were taken and analyzed at various time intervals. Conditions were examined: initial pH range (2, 5, 3, 4, 5, 7, 8, 9, 10) initial CIP concentration (2, 5, 10, 15 mg/L), Ag-NPs dose (0.1, 0.25, 0.75, 1 g/L) and temperature (20, 30, 40, 50° C) were considered. Eq. (1) has been used to determine the performance of CIP removal.

1. Effect of Ag-NPs dose

The adsorbent dose is an important parameter because it determines the capacity of the sorbent for a specific initial

adsorbate concentration. Fig.5 demonstrates the effect of the Ag-NPs doses on ciprofloxacin removal. It can be shown that the percentage removal of CIP increased from 18.7%, 25.8%, 33.2%, 40.2%, to 45% by using Ag-NPs as the adsorption dosage increased from 0.1, 0.25, 0.5, 0.75 to 1.0 g/L. The removal rate and effectiveness increased with higher Ag-NPs for adsorption of CIP with keeping the other parameter (pH, drug concentration, contact time, and temperature). This is due to the total area and the active site increased [34]. Also, due to the increase in the number of porous and volume of their porous in the surface of nanoparticles [43]. The dosage of 1g/L was chosen as the best value for iron (Ag-NPs) nanoparticles. Similar behavior was noticed by [43].

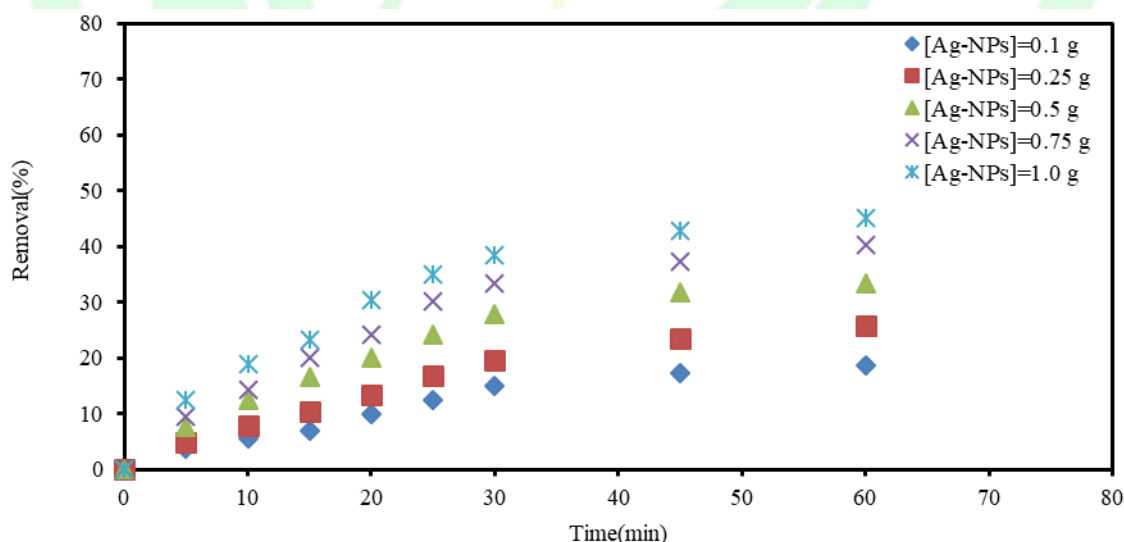


Fig.5: Effect of Ag-NPs doses at pH=3, 10 mg/L CIP, 40°C, 300 rpm, and reaction time 60 min.

2. Effects of initial solution temperatures

Fig.6 explains the percentage removal as a function of temperature in the range of from 20 - 50°C for adsorption of CIP. It can be concluded that temperature has affected the percentage removal of CIP and this removal increased at the temperature increases [37], since values of 20, 30, 40, and 50°C obtained removal percentages of 32.6%, 40.2%, 52%, and 45%, respectively by Ag-NPs, in Fig.6 it can be observed at the temperature increased from 20 to 40°C while at 50°C the removal efficiency decreased. This could be caused by the decrease of viscosity at a temperature increase, which increases pollutant mobility by increasing the diffusion rates of the CIP across the external boundary layer of the sorbent and increasing sorption. Therefore, the number of drugs that interacted with sorbent surface active sites is increased. Also, increasing the temperature will breadth of pore size or activate the sorbent surface or creation of some new active sites on the sorbent surface due to breaking the bonds [27], [11]. Similar observations were noticed by [37]

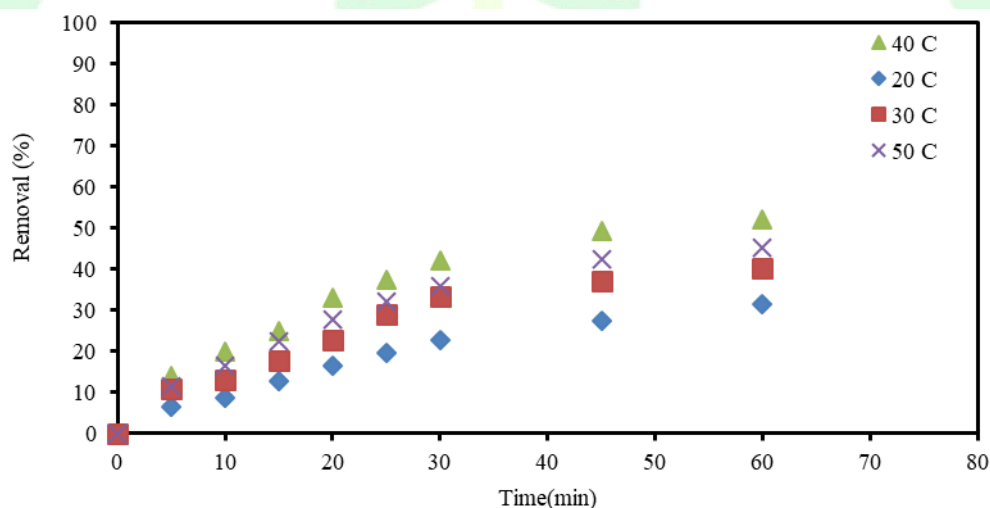


Fig.6: Effect of temperature for removal efficiency of CIP onto various adsorbent at 10 mg/L of CIP, 300 rpm, 60 min, 1 g/L, and pH4 of Ag-NPs

3. Effect of initial pH of the solution

The solution's acidity is the main parameter for controlling CIP adsorption from wastewater. The degree of ionization, the surface load of the sorbent, and the adsorbate classes can be influenced by the pH value. An increase in the pH enhances the most metal sorption to a certain value, followed by a reduction when the pH was further increased. Fig.7 shows the percentage removal of CIP by Ag-NPs within sixty-minute increased at acidic pH and then decreased at basic pH as 37.9%, 45.1%, 52%, 48%, 43.5%, 30.9%, 23.5, and 22%. The best value of pH for removal of CIP by Ag-NPs was pH4. Similar behavior was noticed by [36].

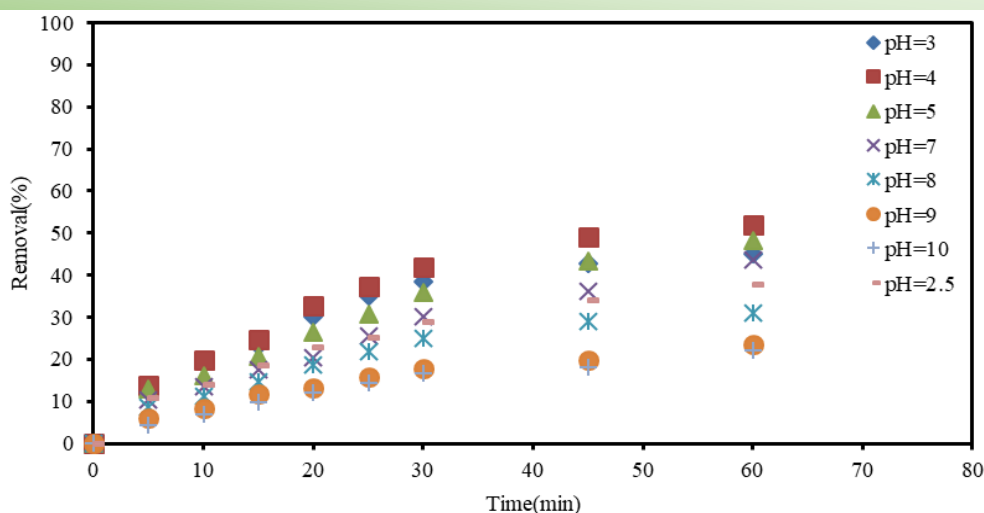


Fig.7: The effect of pH on the removal efficiency of CIP at 10 mg/L of initial concentration, 60 min, and 300 rpm onto 1 g/L, and 40°C of Ag-NPs.

4. Effect of initial concentration

Fig.8 explains the percentage removal as a function of initial drug (CIP) concentrations in the range of from 2-15mg/L for adsorption of CIP. When the initial concentration of CIP increased, the removal efficiency decreased as from 57.7%, 54.6%, 52%, to 48% with sixty minutes, by using Ag-NPs. The possible cause is the initial CIP concentration values for more active sites of the Ag-NPs as they are likely to increase and lead to competitive adsorption of CIP molecules [44]. High initial concentration accelerates the driving force and reduces the mass transfer resistance. The best value of the initial concentration of the CIP with all adsorbent was 10mg/L and the removal efficiency obtained at this concentration was 52% within sixty minutes of the reaction.

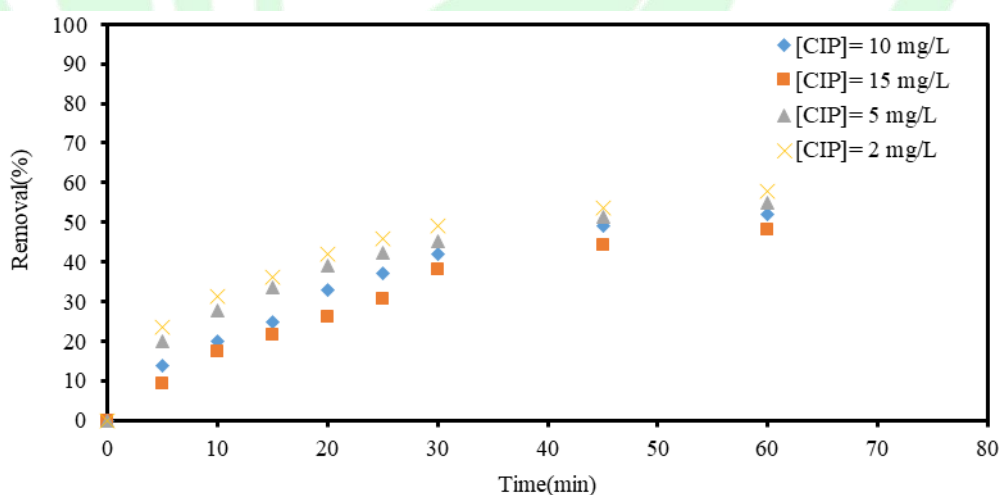


Fig.8: The effect of the initial CIP concentration at 300rpm, 60 min, and Temp=40°C, at adsorbent dose Ag-NPs of 1g/L, pH4.

5. Effect of contact time

The need to identify the possibility of binding and determining the optimal time for sites occupied by drug CIP and completing the removal of the CIP studied lead to the need to study the effect of contact time. Fig.9 shows the influence of increased contact time at pH 4, 7, and 10. The CIP removal efficiency in the batch system increases with additional contact time. The adsorption process was initially rapid due to the driving force of the highest CIP level, after which the removal rate slowed for all pH values because of the continuous decrease in the adsorbent active site and the concentration of non-adsorbed CIP molecules [43]. The CIP removal efficiency at pH 4, 7, and 10 for 60 minutes were 52.5%, 43.5%, and 22% by using Ag-NPs. The CIP removal efficiency after 180 minutes at 4, 7, and 10 were 79.8%, 68%, and 42.2% with Ag-NPs. Similar behavior was noticed by [43].

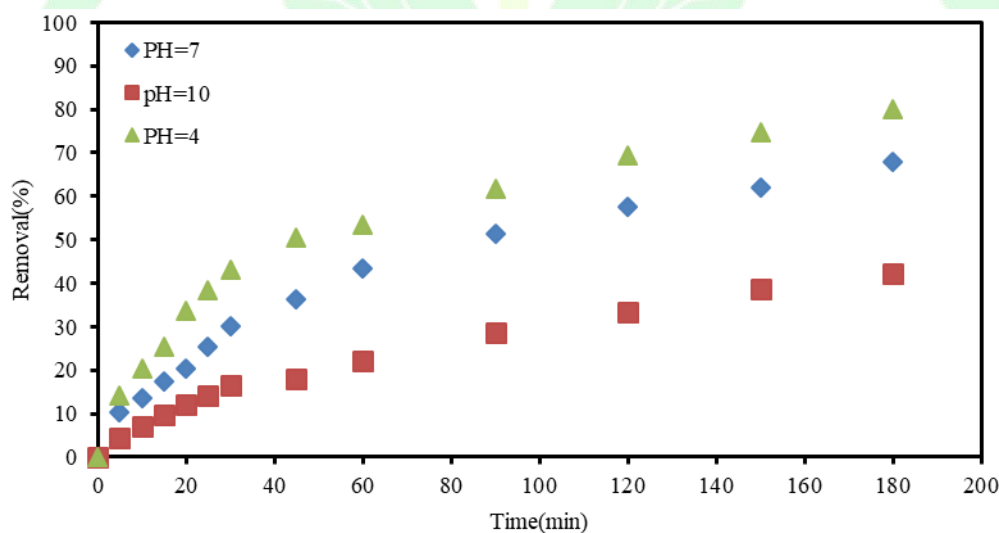


Fig.9: The effect of time at various pH. Experimental conditions: 10 mg/L of CIP, 1 g/L Ag-NPs, with temperature 40°C.

Adsorption Kinetics of silver nanoparticles (Ag-NPs)

The adsorption kinetics studies were performed to investigate the sorption rate. The experiments were carried out at sorbent dose (1g/L) for sorption of CIP with pH 4 at different initial CIP concentrations (2, 5, 10, and 15 mg/L) for different time intervals at 40°C

temperature. The linear forms of the pseudo-first-order, the pseudo-second-order [24], [25], [26]. Elovich [27][28]. and Behnajady-Modirshahla-Ghanbary (BMG) models [29] are bellowed.

Pseudo-first-order model

$$\text{Log } (q_e - q_t) = \text{log } q_e - k_1 t / 2.303 \dots\dots\dots (3)$$

pseudo-second-order model

$$t / q_t = 1/k_2 q_e^2 + t / q_e \dots\dots\dots (4)$$

$$h = K^2 q_e^2 \dots\dots\dots (5)$$

Elovich-model

$$q_t = 1/\beta \ln(\alpha\beta) + 1/\beta \ln(t) \dots\dots\dots (6)$$

Behnajady-Modirshahla-

Ghanbary (BMG) -model

$$t / [1 - (C_t/C_0)] = m + b(t) \dots\dots\dots (7)$$

1. Pseudo-first-order model

Fig.10 explains the linear plot for the Ag-NPs pseudo-first-order model for each factor with a range of (2-15) mg/L, Ag-NPs (0.1 to 1 g/L) dose, pH (2.5 to 10), temperature (20 to 50°C) and time (0 to 60 min). The silver nanoparticles model parameters with the determination

coefficient for each factor are listed in Tables 3. The constant rate k_1 (min^{-1}) was calculated from the slope of the $\log(q_e - q_t)$ and the t graph, as shown in Fig.10. The rate constant (k_1) decreased with the increase of the initial CIP concentration. These results due to the driving force of drug adsorption to the inside structure of the adsorbent used[45]. k_1 (rate constant for first order $>$ k_2 for second-order) for all factors as shown in Table 3 and the best-fit equation for CIP kinetic adsorption to Ag-NPs was the pseudo-first-order. As observed in Table 3, the pseudo-first-order kinetic model is best, as it has an average regression coefficient R^2 values were 0.9813 higher than other kinetic models. A similar observation was noticed by [26], [27].

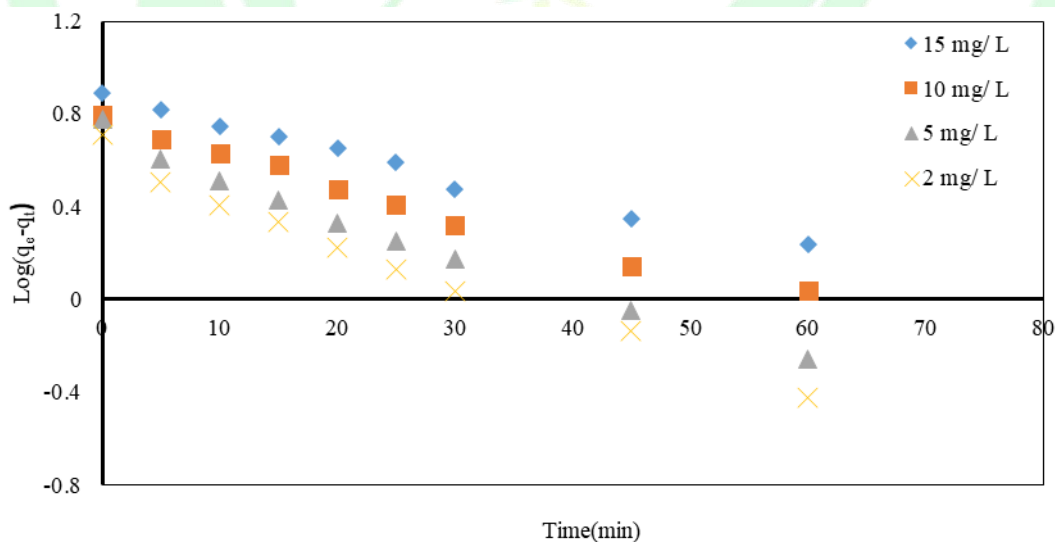


Fig.10: The Pseudo-first-order model of Ag-NPs at different CIP concentration (2-15 mg/L), at 300 rpm, 60 min, Temp=40°C, at adsorbent dose Ag-NPs of 1g/L, and pH4.

2. pseudo-second-order model

The pseudo-second-order model is illustrated by Fig.11 for the adsorption of CIP at different initial CIP concentration range 2mg/L to 15 mg/L. The model parameters and the corresponding coefficient of correlation are shown in Table 3. The rate constants k_2 and q_e were calculated from the intercept and slope of t/q_t versus the t graph Fig.11. In equation (5), the initial adsorption constant rate (h) was estimated from the pseudo-second-order. The values of h (mg/g min^{-1}) for the fixed concentration of CIP (15mg/L, 10mg/L, 5 mg/L and 2mg/L) was (0.3698, 0.4074, 0.6847, 0.6795), and small k_2 values parallel to h indicated rapid sorption at the beginning, followed by slower adsorption. Fig.11 shown as a supplementary information.

3. Elovich model

α (mg/g/min) adsorption value and β (g/mg) desorption rates constants as shown in Fig.12 were obtained from the intercept and slope of q_t against $\ln(t)$. The α and β values of (15, 10, 5, and 2 mg/L) were (0.8968, 0.8824, 1.2145, and 1.1471) and (0.6559, 0.75907, 0.7391, and 0.861), by using Ag-NPs as shown in Table 3, this results showed a higher rate of adsorption than desorption with the initial CIP

concentration, and the regression coefficient was 0.9458. Fig.12 shown as a supplementary information.

4. Behnajady-Modirshahla-Ghanbary (BMG) models

The BMG kinetic model parameters m (min) and b for CIP adsorption under various conditions were calculated from a slope and intercept of $t/[1-(C_t/C_0)]$ against t as shown in Fig.13. As the concentration of CIP increased from (2 to 15 mg/L), the values of m and b increased from (12.091 and 1.6031 to 33.962 and 1.6181), by using Ag-NPs, respectively. This indicates that the time of the adsorption reaction increased when the concentration of CIP increased, as shown in Table 3. As observed in Table 3 the pseudo-first-order kinetic model is best, as it has a regression coefficient R^2 value (0.9813) at various initial concentrations higher than other kinetic models. Such deviations have already been noted in numerous research papers [34], and [26], while in other research paper the second-order was the best model as [46], and [31]. Fig.13 shown as a supplementary information.

CIP mg/L	R% After 60 min	Pseudo-first-order			Pseudo-second-order			Elovichs – Model			BMG- Model		
		q _e (mg g ⁻¹)	k ₁ (min ⁻¹)	R ²	q _e (mg g ⁻¹)	k ₂ (g mg ⁻¹ min ⁻¹)	R ²	α (mg g ⁻¹ min ⁻¹)	β (g mg ⁻¹)	R ²	m (min)	b	R ²
15	48%	7.3705	0.0255	0.9848	7.7639	0.0061	0.820 8	0.8968	0.6559	0.9169	33.962	1.618 1	0.8208
10	52%	5.7003	0.0297	0.9813	6.2695	0.0103	0.890 6	0.8824	0.759	0.9458	24.449	1.589	0.8906
5	54.6%	4.9396	0.0379	0.9852	6.0168	0.0189	0.963 2	1.2145	0.7391	0.995	14.561	1.657 4	0.9632
2	57.7%	4.056	0.0405	0.9801	5.1255	0.0258	0.971 4	1.1471	0.861	0.9969	12.091	1.603 1	0.9714
Average R²				0.9828	0.911 5			0.9636			0.9115		

Table 3: The Pseudo-first-order, Pseudo-Second-order, Elovich, and MBG Kinetics parameters for the adsorption of CIP onto Ag-NPs at various initial concentrations of CIP.

Adsorption mechanism of silver nanoparticle (Ag-NPs)

Equations (8) and (9) determined the adsorption process mechanism [46], [43], [30]. Fig.15a-b presents the intraparticle diffusion kinetic model and the liquid film diffusion of CIP sorption onto Ag-NPs, and the parameter values are given in Table 4. The intraparticle constant (K_{id}) values increase as the initial concentration of CIP concentration increased, indicating a higher sorption rate at a higher initial

concentration of CIP. The positive values of C constants for CIP suggest a boundary layer effect on the sorption rate. K_{id} (mg/g min^{0.5}) and C (mg/g) are the intraparticle diffusion constants. The C parameter indicates the thickness of the boundary layer [43], and K_{fd} (m⁻¹) is the liquid film diffusion constant. When the linear trend line fit from the q_t vs t^{0.5} point Fig.14.a is passing or close to the point of origin of the parameter C=0; thus the limiting rate is intraparticle diffusion. The slope and intercept of the plot of ln (1-q_t/q_e) versus t

in Fig.14.b relate to K_{fd} and C . In Table 4 the high regression coefficient values suggest that the liquid film diffusion is more applicable, and the main controlling step of the higher concentration gradient results in a higher rate of CIP molecule diffusion through the boundary layer surrounding the adsorbent. [27], [30].

Fig.14a, b shown as a supplementary information.

$$q_t = K_{id} t^{1/2} + C \dots\dots\dots (8)$$

$$\ln (1 - q_t / q_e) = -K_{fd} t \dots\dots\dots (9)$$

Table 4: The adsorption mechanism of intraparticle - model and Liquid Film diffusion at the various initial concentration of CIP onto Ag-NPs.

CIP (mg/L)	Intraparticle diffusion			Liquid Film diffusion		
	$K_{id}(\text{mg/g.min}^{0.5})$	$C(\text{mg/g})$	R^2	$K_{fd} (\text{min}^{-1})$	$C(\text{mg/g})$	R^2
15	0.8465	-0.358	0.979	0.0257	-0.0521	0.9848
10	0.7216	-0.0958	0.9826	0.0298	-0.0952	0.9813
5	0.719	0.3928	0.9731	0.0681	-0.1973	0.9852
2	0.6123	0.4693	0.9594	0.0405	-0.2339	0.9801
Average R^2			0.9735			0.9828

Adsorption Isotherm of silver nanoparticles (Ag-NPs)

The adsorption isotherms, which are the important requirements for the development of adsorption systems, depending on the equilibrium data. In this study the equilibrium data for the CIP of the Ag-NPs were modeled on four different isothermal equations: Langmuir, Freundlich, Temkin, and Dubinin that are

linearized forms Eqs. (10)to (16) as shown below [30][31], [24].

Langmuir isotherm model

$$1/q_e = 1/q_{max} k_L (1/C_e) + 1/q_{max} \dots\dots\dots (10)$$

$$R_L = 1 / (1 + bC_0) \dots\dots\dots (11)$$

Freundlich isotherm model

$$\text{Log } q_e = (1/n) \log C_e + \log K_F \dots\dots\dots (12)$$

Temkin-isotherm model

$$q_e = (RT/B_T) \ln C_e + (RT/B_T) \ln K_T \dots\dots\dots (13)$$

Dubinin isotherm model

$$\ln q_e = \ln q_m - \beta \epsilon^2 \dots\dots\dots (14)$$

$$\epsilon = RT \ln (1+1/C_e) \dots\dots\dots (15)$$

$$E = 1/\sqrt{-2\beta} \dots\dots\dots (16)$$

1. Langmuir model

Fig.15 explain the linear plot of this model, where k_L and q_{max} are Langmuir constants. These values were determined from the slope and intercept of the plotted graph $1/q_e$, versus $1/C_e$. Langmuir isotherms defined the results where (R^2) Freundlich is higher than Langmuir models, and heterogeneous adsorbent surfaces with the same adsorption sites should be in Freundlich as shown in Tables 5. The Langmuir constant b was established at 0.3634Lmg^{-1} for Ag-NPs as shown in Table 5. The values of R_L obtained for CIP adsorption on Ag-NPs were in the range (0.2504-0.1793) it showed favorable adsorption of CIP onto adsorbents for the R_L values. The

maximum uptake (q_{max}) was 8.5034mg of CIP per gram of the Ag-NPs. The Dubinin model was the best-fitted model. Similar behavior was noticed by [24]. Fig.15 shown as a supplementary information.

2. Freundlich isotherm model

Fig.16 demonstrates the linear plot of the Freundlich model, this model suggests that the adsorption process showed by a multilayer adsorption mechanism on a heterogeneous adsorbent surface [31]. The values k_F and n are Freundlich coefficients, and confirm that favorable sorption was determined from the slope and intercept of the plotted graph $\log q_e$ versus $\log C_e$ as shown in Fig.16. The n constants influence the adsorption favorability, and the values of n for 2 to 10 are generally good, where the value of n was 2.7078 as shown in Table 5 [46]. Fig.16 shown as a supplementary information.

3. Temkin isotherm model

Fig.17 explain the linear plot of this model. The K_T and B_T values were determined from the slope and intercept of a plotted q_e graph, versus $\ln C_e$ Figure (4.50), K_T (L/g) and B_T (kJ/mol) are coefficients of the maximum binding energy and heat of sorption. The K_T and B_T values in Table 5 define minute variations in sorption heat and robust

interactions between adsorbate and adsorbent. The parameters of the model along with the corresponding correlation coefficient are listed in Table 5 and we can notice applicability of this model according to the high correlation coefficient R^2 . Fig.17 shown as a supplementary information.

4. Dubinin isotherm model

Table 5 shows the parameters of this model q_e and β degree and average

sorption energy per mole of adsorbate, which can be measured from the intercept and slope of the graph plotted $\ln q_e$ versus ϵ^2 Fig.18. From Eq.16, the E values were (3.8727 kJ/ mol) for Ag-NPs, which indicates physical adsorption $E < 8$ kJ/ mol. The value of R^2 (0.9907) is higher than other models for Ag-NPs adsorbent, so it is the best-fitted model. Fig.18 shown as a supplementary information.

Table 5: Isotherm parameters values of Ag-NPs

Langmuir			Freundlich		
$q_{max} (mg\ g^{-1})$	$B (L\ mg^{-1})$	R^2	k_F	n	R^2
8.5034	0.3634	0.9032	3.0134	2.7078	0.907
Temkin			Dubinin		
$K_T (L/g)$	$B_T (kJ/mol)$	R^2	$q_m (\mu g/g)$	$E (kJ/mol)$	R^2
0.1673	3.1553	0.9081	1.0325	3.8727	0.9907

Adsorption Thermodynamic

Thermodynamic parameters of enthalpy; entropy, and Gibbs free energy were calculated from equations (17) to (19)[27], [31], [24], [30]. The adsorption thermodynamic was carried at 298, 303, 313, and 323C. The Gibbs free energy (ΔG^0) was computed using $\ln K_c$ values for dissimilar temperatures. According to Eq.(19), enthalpy (ΔH^0) and entropy (ΔS^0) can be estimated from the intercept and slope at ΔH^0 and ΔS^0 of the plot of ΔG^0 , versus the T Fig.19-a. The free energy, enthalpy, and entropy values are given in Table 6. The negative free energy suggesting the spontaneous nature of CIP adsorption onto Ag-NPs [30]. The positive enthalpy value showed favorable and endothermic sorption, positive entropy implied the increased randomness at the solid-solution interface during the adsorption of

CIP[30], [31]. According to Eq.(21), the activation energy was calculated [24]. These values were calculated by the slope and intercept of $\ln (C_t/C_0)$ and time t (min). The straight line of $\ln k_{obs}$ against $1/T$ Fig.19-b deviated by 14.06 kJ/mol indicating diffusion-controlled processes. Fig.19a, b shown as a supplementary information.

$$\Delta G^0 = -RT \ln K_c \tag{17}$$

$$K_c = q_e / C_e \tag{18}$$

$$\Delta G^0 = \Delta H^0 - T\Delta S^0 \tag{19}$$

$$\ln (C_t / C_0) = -k_{obs} t \tag{20}$$

$$\ln k_{obs} = \ln A - E_a / RT \tag{21}$$

Table (6): Thermodynamic examination of the adsorption of CIP onto Ag-NPs(initial concentration 10 mg/L, Ag-NPs dose 1g/L, contact time 60 min, agitation speed 300 rpm, and pH=4).

ΔG^0 (kJ/mol)				ΔH^0 (kJ/mol)	ΔS^0 (kJ/mol.K)
T=20°C	T=30°C	T=40°C	T=50°C	12.713	0.0422
0.5163	-0.0691	-0.9589	-0.5927		

CONCLUSION

This study examined the adsorption of CIP adsorption by Ag-NPs in a batch system. The characterisation of the adsorbent was carried out with advanced SEM, AFM, BET, Zeta Potentials and FT-IR, and the result indicates:

1. pH4, 60 min, 10 mg/L, 40 °C, and 1 g/L have been used to optimize process adsorption parameters with

pH, contact time, initial antibiotic concentration and temperature.

2. The studies were performed in isothermal, kinetic, and thermodynamic with optimal effect data.
3. The isothermal study has shown that the surface of Ag-NPs consists of homogenous sites ready for antibiotic reactions.

4. The thermodynamic element highlighted the spontaneous and endothermic nature of adsorption.
5. The impact of agitation speed, nanoparticle size and magnetic bar sizes on the first-order adsorption of Ag-NPs should be taken into account in future studies and kinetic physical adsorption should be established for this purpose.

REFERENCES

- [1]V. M. F. Frade, M. Dias, A. C. S. C. Teixeira, and M. S. A. Palma (2014) Environmental contamination by fluoroquinolones, *Brazilian J. Pharm. Sci.*, vol. 50, no. 1, pp. 41–54, doi: 10.1590/s1984-82502011000100004.
- [2]M. S. Gasser, H. T. Mohsen, and H. F. Aly(2008) Humic acid adsorption onto Mg/Fe layered double hydroxide, *Colloids Surfaces A Physicochem. Eng. Asp.*, vol. 331, no. 3, pp. 195–201, 2008, doi: 10.1016/j.colsurfa..08.002.
- [3]W. Da Oh, V. W. C. Chang, and T. T. Lim (2017) A comprehensive performance evaluation of heterogeneous Bi₂Fe₄O₉/peroxymonosulfate system for sulfamethoxazole degradation, *Environ. Sci. Pollut. Res.*, vol. 26, no. 2, pp. 1026–1035, doi: 10.1007/s11356-017-8476-9.
- [4]Y. Ji, C. Ferronato, A. Salvador, X. Yang, and J.-M. Chovelon (2013) Degradation of ciprofloxacin and sulfamethoxazole by ferrous-activated persulfate: Implications for remediation of groundwater contaminated by antibiotics, *Sci. Total Environ.*, vol. 472, pp. 800–808, doi: <https://doi.org/10.1016/j.scitotenv.11.008>.
- [5]E. M. Kalhori, E. Ghahramani, T. J. Al-Musawi, H. N. Saleh, M. N. Sepehr, and M. Zarrabi (2018) Effective reduction of metronidazole over the cryptomelane-type manganese oxide octahedral molecular sieve (K-OMS-2) catalyst: facile synthesis, experimental design and modeling, statistical analysis, and identification of by-products, *Environ. Sci. Pollut. Res.*, vol. 25, no. 34, pp. 34164–34180, doi: 10.1007/s11356-018-3352-9.
- [6]M. S. Legnoverde, S. Simonetti, and E. I. Basaldella (2014) Influence of pH on cephalexin adsorption onto SBA-15 mesoporous silica: Theoretical and experimental study, *Appl. Surf. Sci.*, vol. 300, pp. 37–42, 2014, doi: 10.1016/j.apsusc..01.198.
- [7]M. M. Soori, E. Ghahramani, H. Kazemian, T. J. Al-Musawi, and M. Zarrabi(2016) “Intercalation of tetracycline in nano sheet layered

- double hydroxide: An insight into UV/VIS spectra analysis, *J. Taiwan Inst. Chem. Eng.*, vol. 63, pp. 271–285, doi: 10.1016/j.jtice.2016.03.015.
- [8] X. Huang, J. Zheng, C. Liu, L. Liu, Y. Liu, and H. Fan (2017) Removal of antibiotics and resistance genes from swine wastewater using vertical flow constructed wetlands: Effect of hydraulic flow direction and substrate type, *Chem. Eng. J.*, vol. 308, pp. 692–699, doi: 10.1016/j.cej.2016.09.110.
- [9] M. R. Samarghandi, T. J. Al-Musawi, A. Mohseni-Bandpi, and M. Zarrabi (2015) Adsorption of cephalexin from aqueous solution using natural zeolite and zeolite coated with manganese oxide nanoparticles, *J. Mol. Liq.*, vol. 211, pp. 431–441, doi: 10.1016/j.molliq.06.067.
- [10] A. A. Mohammed and S. L. Kareem (2019) Adsorption of tetracycline from wastewater by using Pistachio shell coated with ZnO nanoparticles: Equilibrium, kinetic and isotherm studies, *Alexandria Eng. J.*, vol. 58, no. 3, pp. 917–928, doi: 10.1016/j.aej.2019.08.006.
- [11] A. A. Mohammed, T. J. Al-Musawi, S. L. Kareem, M. Zarrabi, and A. M. Al-Ma'abreh (2019) Simultaneous adsorption of tetracycline, amoxicillin, and ciprofloxacin by pistachio shell powder coated with zinc oxide nanoparticles, *Arab. J. Chem.*, doi: 10.1016/j.arabjc.2019.10.010.
- [12] S. K. Bajpai, M. Bajpai, and N. Rai (2012) Sorptive removal of ciprofloxacin hydrochloride from simulated wastewater using sawdust: Kinetic study and effect of pH, *Water SA*, vol. 38, no. 5, pp. 673–682, doi: 10.4314/wsa.v38i5.4.
- [13] H. R. Pouretedal and N. Sadegh (2014) Effective removal of Amoxicillin, Cephalexin, Tetracycline and Penicillin G from aqueous solutions using activated carbon nanoparticles prepared from vine wood, *J. Water Process Eng.*, vol. 1, pp. 64–73, doi: 10.1016/j.jwpe.2014.03.006.
- [14] K. Bondarczuk and Z. Piotrowska-Seget (2018) Microbial diversity and antibiotic resistance in a final effluent-receiving lake, *Sci. Total Environ.*, vol. 650, pp. 2951–2961, 2019, doi: 10.1016/j.scitotenv.10.050.
- [15] Z. Q. Shi, Y. S. Liu, Q. Xiong, W. W. Cai, and G. G. Ying (2019) Occurrence, toxicity and transformation of six typical benzotriazoles in the environment: A review, *Sci. Total Environ.*, vol. 661, pp. 407–421, 2019, doi: 10.1016/j.scitotenv.01.138.
- [16] Q. Xian, L. Hu, H. Chen, Z. Chang,

- and H. Zou (2010) Removal of nutrients and veterinary antibiotics from swine wastewater by a constructed macrophyte floating bed system, *J. Environ. Manage.*, vol. 91, pp. 2657–2661, doi: 10.1016/j.jenvman.07.036.
- [17] O. F. Ahalya, Chemistry and T. V Ramachandra (2003) Biosorption of Heavy Metals Biosorption of Heavy Metals, *Res. J. Chem. Environ.*, vol. 7, no. 4, pp. 71–79.
- [18] C. Zou, W. Jiang, J. Liang, X. Sun, and Y. Guan (2019) Removal of Pb(II) from aqueous solutions by adsorption on magnetic bentonite, *Environ. Sci. Pollut. Res.*, vol. 26, no. 2, pp. 1315–1322, doi: 10.1007/s11356-018-3652-0.
- [19] J. Singh, T. Singh, and M. Rawat (2017) Green synthesis of silver nanoparticles via various plant extracts for anti-cancer applications, *Glob. J. nanomedicine*, vol. 2, no. 3, pp. 2–5, [Online]. Available: <https://juniperpublishers.com/gjn/pdf/GJN.MS.ID.555590.pdf>.
- [20] H. Noritomi, Y. Umezawa, S. Miyagawa, and S. Kato (2011) Preparation of Highly Concentrated Silver Nanoparticles in Reverse Micelles of Sucrose Fatty Acid Esters through Solid-Liquid Extraction Method, *Adv. Chem. Eng. Sci.*, vol. 01, no. 04, pp. 299–304, doi: 10.4236/aces.14041.
- [21] Y. Delgado-Beleño, C. E. Martinez-Nuñez, M. Cortez-Valadez, N. S. Flores-López, and M. Flores-Acosta (2012) Optical properties of silver, silver sulfide and silver selenide nanoparticles and antibacterial applications, *Mater. Res. Bull.*, vol. 99, pp. 385–392, doi: 10.1016/j.materresbull.11.015.
- [22] J. D. Oei *et al.* (2012) Antimicrobial acrylic materials with in situ generated silver nanoparticles, *J. Biomed. Mater. Res. - Part B Appl. Biomater.*, vol. 100 B, no. 2, pp. 409–415, doi: 10.1002/jbm.b.31963.
- [23] A. Tlili, J. Jabiol, R. Behra, C. Gil-Allué, and M. O. Gessner (2017) Chronic Exposure Effects of Silver Nanoparticles on Stream Microbial Decomposer Communities and Ecosystem Functions, *Environ. Sci. Technol.*, vol. 51, no. 4, pp. 2447–2455, doi: 10.1021/acs.est.6b05508.
- [24] Y. Li, Q. Yue, B. Gao, Q. Li, and C. Li (2008) Adsorption thermodynamic and kinetic studies of dissolved chromium onto humic acids, *Colloids Surfaces B Biointerfaces*, vol. 65, no. 1, pp. 25–29, doi: 10.1016/j.colsurfb.2008.02.014.
- [25] T. Jiao *et al.*, (2015) Reduced Graphene Oxide-Based Silver

- Nanoparticle-Containing Composite Hydrogel as Highly Efficient Dye Catalysts for Wastewater Treatment, *Sci. Rep.*, vol. 5, no. March, pp. 1–12, doi: 10.1038/srep11873.
- [26] C. Hou *et al.*, (2016) Preparation and dye removal capacities of porous silver nanoparticle-containing composite hydrogels: Via poly(acrylic acid) and silver ions, *RSC Adv.*, vol. 6, no. 112, pp. 110799–110807, doi: 10.1039/c6ra23371f.
- [27] A. M. Aljeboree, A. N. Alshirifi, and A. F. Alkaim (2014) Kinetics and equilibrium study for the adsorption of textile dyes on coconut shell activated carbon, *Arab. J. Chem.*, doi: 10.1016/j.arabjc.01.020.
- [28] I. Ali, Z. A. Al-Othman, and A. Alwarthan (2016) Synthesis of composite iron nano adsorbent and removal of ibuprofen drug residue from water, *J. Mol. Liq.*, vol. 219, pp. 858–864, 2016, doi: 10.1016/j.molliq.2016.04.031.
- [29] A. K. Hassan, M. M. Rahman, G. Chattopadhyay, and R. Naidu (2019) Kinetic of the degradation of sulfanilic acid azochromotrop (SPADNS) by Fenton process coupled with ultrasonic irradiation or L-cysteine acceleration, *Environ. Technol. Innov.*, vol. 15, p. 100380, doi: 10.1016/j.eti..100380.
- [30] M. Ghaedi, B. Sadeghian, A. A. Pebdani, R. Sahraei, A. Daneshfar, and C. Duran (2012) Kinetics, thermodynamics and equilibrium evaluation of direct yellow 12 removal by adsorption onto silver nanoparticles loaded activated carbon, *Chem. Eng. J.*, vol. 187, pp. 133–141, doi: 10.1016/j.cej.01.111.
- [31] F. Bouhamed, Z. Elouear, and J. Bouzid, (2012) Adsorptive removal of copper(II) from aqueous solutions on activated carbon prepared from Tunisian date stones: Equilibrium, kinetics and thermodynamics, *J. Taiwan Inst. Chem. Eng.*, vol. 43, no. 5, pp. 741–749, doi: 10.1016/j.jtice.02.011.
- [32] A. W. Qassim (2015) Spectrophotometric Determination of Ciprofloxacin Hydrochloride InPharmaceutical Formulation Ciproxin, *Int. J. Adv. Sci. Tech. Res.*, vol. 3, no. 5, pp. 135–146.
- [33] N. Sharma and N. Dhiman (2017) Kinetic and Thermodynamic Studies for Ciprofloxacin Hydrochloride Adsorption from Aqueous Solution on CuO Nanoparticles, vol. 10, no. 5, pp. 98–106.
- [34] M. A. Asghar *et al.*, (2018) Iron, copper and silver nanoparticles: Green synthesis using green and black tea leaves extracts and evaluation of

- antibacterial, antifungal and aflatoxin B1 adsorption activity, *LWT - Food Sci. Technol.*, vol. 90, no. January, pp. 98–107, doi: 10.1016/j.lwt.12.009.
- [35] S. Raj, S. Chand Mali, and R. Trivedim (2018) Green synthesis and characterization of silver nanoparticles using *Enicostemma axillare* (Lam.) leaf extract, *Biochem. Biophys. Res. Commun.*, vol. 503, no. 4, pp. 2814–2819, doi: 10.1016/j.bbrc.08.045.
- [36] F. Zia, N. Ghafoor, M. Iqbal, and S. Mehboob (2016) Green synthesis and characterization of silver nanoparticles using *Cydonia oblong* seed extract, *Appl. Nanosci.*, vol. 6, no. 7, pp. 1023–1029, doi: 10.1007/s13204-016-0517-z.
- [37] E. Hiba (2018) Green synthesis of silver nanoparticles using *Lawsonia inermis* leaves extract and its antibacterial activity Email : Hmk20001999@gmail.com Chemistry Department , College of Science , University of,” vol. 13, no. 2, pp. 102–118.
- [38] D. Aksu Demirezen, Y. Ş. Yıldız, and D. Demirezen Yılmaz (2019) Amoxicillin degradation using green synthesized iron oxide nanoparticles: Kinetics and mechanism analysis, *Environ. Nanotechnology, Monit. Manag.*, vol. 11, no. September, doi: 10.1016/j.enmm.100219.
- [39] N. Khoshnamvand, S. Ahmadi, and F. K. Mostafapour (2017) Kinetic and isotherm studies on ciprofloxacin an adsorption using magnesium oxide nanoparticles, *J. Appl. Pharm. Sci.*, vol. 7, no. 11, pp. 79–83, doi: 10.7324/JAPS.2017.71112.
- [40] Y. Y. Loo, B. W. Chieng, M. Nishibuchi, and S. Radu, “Synthesis of silver nanoparticles by using tea leaf extract from *Camellia Sinensis*,” *Int. J. Nanomedicine*, vol. 7, pp. 4263–4267, doi: 10.2147/IJN.S33344.
- [41] W. R. Rolim *et al.*, (2019) Green tea extract mediated biogenic synthesis of silver nanoparticles: Characterization, cytotoxicity evaluation and antibacterial activity, *Appl. Surf. Sci.*, vol. 463, no. May, pp. 66–74, doi: 10.1016/j.apsusc.2018.08.203.
- [42] K. Jyoti and A. Singh (2016) Green synthesis of nanostructured silver particles and their catalytic application in dye degradation, *J. Genet. Eng. Biotechnol.*, vol. 14, no. 2, pp. 311–317, doi: 10.1016/j.jgeb.09.005.
- [43] M. Ravanan, M. Ghaedi, A. Ansari, F. Taghizadeh, and D. Elhamifar (2014) Comparison of the efficiency of Cu and silver nanoparticle loaded on supports for the removal of Eosin y from aqueous solution: Kinetic and isotherm

- study, *Spectrochim. Acta - Part A Mol. Biomol. Spectrosc.*, vol. 123, pp. 467–472, doi: 10.1016/j.saa..12.049.
- [44] X. Weng, L. Huang, Z. Chen, M. Megharaj, and R. Naidu (2013) Synthesis of iron-based nanoparticles by green tea extract and their degradation of malachite, *Ind. Crops Prod.*, vol. 51, pp. 342–347, doi: 10.1016/j.indcrop.09.024.
- [45] M. Leili, M. Fazlzadeh, and A. Bhatnagar (2017) Green synthesis of nano-zero-valent iron from Nettle and Thyme leaf extracts and their application for the removal of cephalexin antibiotic from aqueous solutions, *Environ. Technol. (United Kingdom)*, vol. 39, no. 9, pp. 1158–1172, doi: 10.1080/09593330.1323956.
- [46] Y. Sun *et al.*, (2013) Adsorption and cosorption of ciprofloxacin and Ni(II) on activated carbon-mechanism study, *J. Taiwan Inst. Chem. Eng.*, vol. 45, no. 2, pp. 681–688, doi: 10.1016/j.jtice..05.013.